Journal of Physics: Condensed Matter

ACCEPTED MANUSCRIPT

Exploring structural, electronic, and mechanical properties of 2D hexagonal MBenes

To cite this article before publication: Rasoul Khaledialidusti *et al* 2020 *J. Phys.: Condens. Matter* in press https://doi.org/10.1088/1361-648X/abbb0e

Manuscript version: Accepted Manuscript

Accepted Manuscript is "the version of the article accepted for publication including all changes made as a result of the peer review process, and which may also include the addition to the article by IOP Publishing of a header, an article ID, a cover sheet and/or an 'Accepted Manuscript' watermark, but excluding any other editing, typesetting or other changes made by IOP Publishing and/or its licensors"

This Accepted Manuscript is **© 2020 IOP Publishing Ltd**.

During the embargo period (the 12 month period from the publication of the Version of Record of this article), the Accepted Manuscript is fully protected by copyright and cannot be reused or reposted elsewhere.
As the Version of Record of this article is going to be / has been published on a subscription basis, this Accepted Manuscript is available for reuse under a CC BY-NC-ND 3.0 licence after the 12 month embargo period.

After the embargo period, everyone is permitted to use copy and redistribute this article for non-commercial purposes only, provided that they adhere to all the terms of the licence https://creativecommons.org/licences/by-nc-nd/3.0

Although reasonable endeavours have been taken to obtain all necessary permissions from third parties to include their copyrighted content within this article, their full citation and copyright line may not be present in this Accepted Manuscript version. Before using any content from this article, please refer to the Version of Record on IOPscience once published for full citation and copyright details, as permissions will likely be required. All third party content is fully copyright protected, unless specifically stated otherwise in the figure caption in the Version of Record.

View the article online for updates and enhancements.

This content was downloaded from IP address 129.241.230.12 on 15/12/2020 at 08:17

Exploring structural, electronic, and mechanical properties of 2D hexagonal MBenes

Rasoul Khaledialidusti,[*a] Mohammad Khazaei,[*b] Vei Wang,[c] Nanxi Miao,[d,e] Chen Si,[f] Jianfeng Wang,[g] Junjie Wang[d,e]

[a]Department of Mechanical and Industrial Engineering, Norwegian University of Science and Technology (NTNU), 7491 Trondheim, Norway. E-mail: rasoul.khaledialidusti@ntnu.no

[b]Department of Physics, Yokohama National University, Yokohama 240-8501, Japan. E-mail: mkhazaei2@gmail.com

[c]Department of Applied Physics, Xi'an University of Technology, Xi'an 710054, China

[d]State Key Laboratory of Solidification Processing, Northwestern Polytechnical University, Xi'an, Shaanxi 710072, People's Republic of China. Email: wang.junjie@nwpu.edu.cn

[e]International Center for Materials Discovery, State Key Laboratory of Solidification Processing, Northwestern Polytechnical University, Xi'an, Shanxi 710072, People's Republic of China

[f]School of Materials Science and Engineering, Beihang University, Beijing 100191, China

[g]Beijing Computational Science Research Center, Beijing 100193, China

A family of two-dimensional (2D) transition metal borides, referred to as MBenes, is recently emerging as novel materials with great potentials in electronic and energy harvesting applications to the field of materials science and technology. Transition metal borides can be synthesized from chemical exfoliation of ternary-layered transition metal borides, known as MAB phases. Previously it has been predicted that thin pristine 2D Sc-, Ti-, Zr-, Hf-, V-, Nb-, Ta-, Mo-, and W-based transition metal borides with hexagonal phase are more stable than their corresponding orthorhombic phase. Here, using a set of first-principles calculations (at absolute zero temperature), we have examined the geometric, dynamic stability, electronic structures, work function, bond strength, and mechanical properties of the hexagonal monolayer of transition metal borides (M = Sc, Ti, Zr, Hf, V, Nb, Ta, Mo, and W) chemically terminated with F, O, and OH. The results of the formation energies of terminated structures imply that the surface terminations could make a strong bond to the surface transition metals and provide the possibility of the development of transition metal borides with those surface terminations. Except for ScBO, which is an indirect bandgap semiconductor, the other transition metal borides are metallic or semimetal. Particularly, TiBF, ZrBF, and HfBF are metallic systems whose band dispersions close to the Fermi level indicate the coexistence of

Accepted Manuscript

type-I and type-II nodal lines. Our calculated work functions indicate that 2D transition metal borides with OH (O) functionalization obtain the lowest (highest) work functions. The results of the mechanical properties of the considered structures imply that oxygen functionalized transition metal borides exhibit the stiffest mechanical strength with 248 < E (N/m) < 348 while non-terminated transition metal borides are generally the weakest systems with 206 < E (N/m) < 283.

1 Introduction

The chemical exfoliation method has opened a way to mass-produce novel 2D materials at a low cost from layered bulk materials that are typically difficult to be prepared directly from pure elements because of their thermodynamic instability compared with their other competitive phases.[1,2] Layered transition metal carbides and nitrides, known as MAX phases, are among the well-known examples of layered materials in which many members were successfully exfoliated into 2D layers of transition metal carbides and nitrides, so-called MXenes, by selective etching of certain atomic layers.[1,2] In detail, in the general chemical formula of conventional MAX phases ($M_{n+1}AX_n$), M represents an early transition metal (Sc, Ti, Zr, Hf, V, Nb, Ta, Cr, and Mo), A is a metal element in group 13 or 14 in the periodic table (*i.e.*, Al, Ga, Si, Ge, Sn, Pb, P, As, Bi, S, Se, and Te), and X is traditionally limited to carbon or nitrogen.[3,4] In MAX phases, the M, A, and X atoms are arranged in a hexagonal close-packed structure.[1,2,5,6] Recently, the family of MAX phases and their derivative 2D MXenes have been expanded to in- and out of plane ordered double transition metals carbides.[7–11] Moreover, there are some experimental and theoretical signs that boron can be used as X element to synthesis MAX phases with nonconventional chemical formula.[12–18] For instance, Ti_2InB_2 with hexagonal symmetry has been first predicted and then synthesized recently.[17] The relatively weaker strength of the M–A bonds than that of the M–X bonds[19] provides a promotion condition to etch the A-layer by chemical treatment to form 2D MXenes.[1] Depending on the type of the utilized acid, e.g., HF acid, the surfaces of MXenes

Accepted Manuscript

are saturated with a mixture of chemical groups, *e.g.*, F, OH, or O.[1] The large family of MAX phases and the derived 2D MXenes have attracted much attention and have widely been studied due to their brilliant chemical and mechanical stabilities. Particularly, MXenes have a unique combination of properties and have been explored in different applications such as electrochemical EMI shielding,[20] wireless communication,[21] membranes,[22] energy storage,[23,24] Li- and Na- ion batteries,[25,26] and catalysts.[27,28]

More recently, some ternary borides as analogous to the MAX phases are familiarized by introducing B as the X element, known as MAB phases.[12–18] Similar to the MAX phases, where the 2D MXenes are obtained by etching of A-element layers, the 2D transition metal borides are made by washing out A elements from the MAB phases, known as MBenes.[12–18] For instance, 2D CrB,[16,18], and MoB[13,14] MBenes were made by etching A-element layers of the MAB phases Cr_2AlB_2 and MoAlB, respectively. 2D MBenes have attracted extensive attention and their electronic and magnetic applications are developing fast. Recent studies introduce 2D MBenes with great potential for applications in Li- and Na-ion batteries,[29–32] electrocatalysis,[13,30] and magnetic devices[33]. Similar to 2D MXenes, various 2D MBenes are expected to be synthesized in the future.

MAB phases possess various chemical formulas (*i.e.*, MAlB, M_2AlB_2, $M_3Al_2B_2$, M_3AlB_4, and M_4AlB_6) and various structural atomic networks with orthorhombic crystals.[15] In MAB phases MAlB, M_2AlB_2, and $M_3Al_2B_2$, boron atoms form one-dimensional isolated zigzag chains perpendicular to the A layer, while double and triple chains of boron atoms connected to create flat strips with hexagonal boron ring networks in M_3AlB_4 and M_4AlB_6, respectively.[15] In our previous study, we investigated the dynamic stabilities and formation energies of many MAB phases (M = Sc, Ti, Zr, Hf, V, Nb, Ta, Cr, Mo, W, Mn, Tc, Fe, Ru, Co, Rh, and Ni) using *ab-initio* calculations.[15] Our results indicated that it is possible to synthesize various MAB phases in the future. In analogous to MAX phases, in some of MAB

Accepted Manuscript

phases, the M-Al bonds are relatively weaker than M-B or B-B bonds. This brings a new opportunity to exfoliate MAB phases to 2D MBenes as evidenced in various experiments. On the basis of total energy and nudged elastic calculations, it was predicted that after exfoliation, 2D MB MBenes with orthorhombic lattices might transform into the hexagonal phase. This structural transformation leads to the rearrangement of boron chains in 2D MB MBenes into a 2D graphene-like boron sheet sandwiched between the metal layers (**Fig. 1**).[15] It was shown that pristine 2D MB MBenes (M = Sc, Ti, Zr, Hf, V, Nb, Ta, Mo, and W) are more stable with hexagonal lattice structures, while 2D MB MBenes are more stable with orthorhombic phases for M = Cr, Mn, Tc, Fe, Ru, and Ni. Therefore, in the future, it may be possible to synthesis MBenes with orthorhombic or hexagonal lattices, or a mixture of these phases in an experimental sample by controlling the environmental conditions. In this study, we have only focused on the electronic structures of hexagonal MBenes.

Similar to MXenes, the surfaces of MBenes are also made of transition metals. Hence, due to the chemical reactivity of transition metals, the surfaces will be terminated with a mixture of F, O, and OH terminations depending on the applied chemical solution.[1,2,34] Here, by using a set of density functional theory calculations, we have systematically investigated the structural stabilities and mechanical properties of the hexagonal monolayer of pristine and functionalized MB MBenes (M = Sc, Ti, Zr, Hf, V, Nb, Ta, Mo, and W) with F, O, or OH groups. At first, we investigate the structural models of 2D MB MBenes systemically. Second, we examine the surface functionalization effect on the formation energies of different MBenes. Then, the dynamical stability of the MBenes is evaluated by calculating the phonon dispersions. Next, we investigate the electronic structures and the effects of surface terminations on the strengths of B–B, M–M, M–B of 2D MB MBenes in the presence or absence of termination groups. The mechanical properties (elastic constants, Poisson's ratio,

Accepted Manuscript

shear modulus, and Young's modulus) of the MBenes are evaluated. Finally, we present the results of the work functions of 2D MB MBenes.

It is worth noting that the double-layers and/or multi-layers of these 2D materials are more feasible to be produced than their monolayers in the experiments. However, the mechanical and electronic properties of these materials insignificantly change between the monolayers and multi-layers of these materials.

It should be noted that the calculations in this paper have been done at zero temperature without including the environmental effects such as the type of acid, its concentration, temperature, or pressure. Surely, these experimental parameters affect the stability and surface functionalization of the 2D MBenes that should be investigated in the future.[35,36]

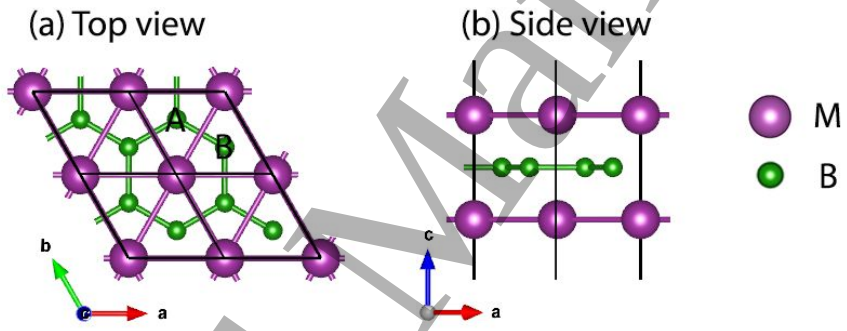

Fig. 1 (a) Top and (b) side views of the hexagonal 2D MB MBene layer. The A-type and B-type hollow sites described in the text are labeled.

2 Computational methods

First-principles calculations based on density functional theory (DFT) were performed using the generalized gradient approximation with the Perdue–Burke–Ernzerhof (PBE)[37] exchange-correlation functional and the projected augmented wave (PAW) approach with a plane-wave cutoff energy of 520 eV, as implemented in the Vienna *ab initio* Simulation Package (VASP).[38] The atomic positions and lattice constants were fully optimized using the conjugate gradient method. The maximum residual force acting on each atom becomes less than 0.0001 eV/Å. The criterion for energy convergence is 10^{-7} eV/cell. For the optimization of 2D MBene structures, 18 × 18 × 1 Monkhorst-Pack *k* points are used.[39] All 2D MBenes

Accepted Manuscript

here were also evaluated using spin-polarized calculations and the results showed that all the studied 2D MBenes are nonmagnetic. The partial occupancies were determined using the Methfessel–Paxton smearing scheme with a smearing width of 0.1 eV.[40] A large vacuum space with a thickness of at least 30 Å was used to avoiding any interaction between an MBene sheet and its periodically repeated images along the *c* axis.

The formation energies $E_{form}^{MBT_x}$ of the MBene nano-sheets were calculated as defined below using the total energies of the 2D MBene structure ($E_{tot}^{MBT_x}$), the total energies of the bulk phases of the composed M and B per atom (E_{tot}^{M}, E_{tot}^{R}), and the total energies per atom of termination group using their stable gas molecules $E_{tot}^{T_x}$. Depending on the type of surface functions, $E_{tot}^{T_x}$ is the half of the total energies of F_2, O_2+H_2, or O_2 and n_{T_x} is 2:

$$E_{form}^{MBT_x} = E_{tot}^{MBT_x} - n_M E_{tot}^{M} - n_B E_{tot}^{R} - n_{T_x} E_{tot}^{T_x} \quad (1)$$

where $n_M$and n_B are the number of atoms in the *M* and *B* unit cells, respectively. In the unit cell of 2D MB MBenes, $n_M$and n_B are equal to 2.

The dynamical stability of the 2D MBene structures was examined using a set of phonon spectra calculations. The phonon is obtained within the Finite-difference Method (FDM) approach using the PHONOPY code[41] combined with VASP[38]. The total energies were converged within 10^{-8} eV/cell to ensure a reasonable convergence. The force constants in the 2D MBene structures were calculated for an isotropic 5 × 5 × 1 supercell whose BZ are sampled with 5 × 5 × 1 Monkhorst-Pack *q* points.[39]

To evaluate a bond strength, we used the 3 × 3 matrix of force constants, which is one of the output results of the phonon calculations. The matrix of force constants was calculated from the finite difference approximation to the first-order derivative of the atomic forces with respect to finite displacements of each pair of atoms along with the Cartesian directions. We

Accepted Manuscript

used the value of trace of the force constant tensor since it has the advantage of being independent of the coordinate system. The force constant F_{ij} between atoms i and j are referred to this scalar quantity.[15,42]

We also employed the crystal orbital Hamilton population (COHP) analysis[43] to evaluate a bond strength. The COHP analysis is a theoretical bond-detecting technique for solids, which partitions the band-structure energy into orbital-pair interactions. More details are given in **Supplementary information**.

For a 2D hexagonal crystal, there are two independent elastic constants, namely, c_{11} and c_{12}. The in-plane stiffness tensor c_{ij} (i,j=1,2) can be obtained based on the following formula in first-principles calculations,

$$E_s = \frac{1}{2}c_{11}\varepsilon_{xx}^2 + \frac{1}{2}c_{22}\varepsilon_{yy}^2 + c_{12}\varepsilon_{xx}\varepsilon_{yy} \quad (2)$$

where E_s is the elastic strain energy, and the tensile strain ε is defined as $\varepsilon = \frac{a-a_0}{a}$, a and a_0 are the lattice constants of the strained and strain-free structures, respectively. Applying uniaxial strain ε along x-direction leads to $\varepsilon_{yy} = 0$ and $E_s = {}^1\!/_2 c_{11}\varepsilon_{xx}^2$. The elastic constant c_{11} can be acquired from the coefficient of the quadratic term by fitting the data of elastic strain energy $E_s(\varepsilon)$ as a function of strain ε using a quadratic polynomial. Similarly, we can obtain c_{12} by fitting the expression $E_s = ({}^1\!/_2 c_{11} + {}^1\!/_2 c_{22} + c_{12})\varepsilon_{xx}^2$ when equibiaxial strain is applied ($\varepsilon_{xx} = \varepsilon_{yy}$). Finally, c_{66} is equal to ${}^1\!/_2(c_{11} - c_{12})$. To calculate the elastic stiffness constants, the E_s as a function of ε in the strain range -1.5% $\leq \varepsilon \leq$ 1.5% with an increment of 0.5% are investigated. A mechanically stable 2D hexagonal sheet would satisfy $c_{11} > 0$ and $c_{11} > |c_{12}|$.

3 Structural models

Accepted Manuscript

As shown in **Fig. 1b**, pristine MB MBene was constructed of three atomic layers with a hexagonal-like unit cell, where a single graphene-like boron layer is sandwiched between the double layers of transition metals. There are two types of hollow sites (*i.e.*, A and B) on the MB surfaces, as shown in **Fig. 1a**. Therefore, depending on the position of the chemical groups on the surface, the stability and consequently the electronic structures may change. Here, we have examined four different configurations for the surface terminations of the MB systems: Model 1 in which two functional groups are located on top of the hollow sites H1 or H2 (**Fig. 2a**); Model 2 in which one functional group is located on top of the hollow site H1 and the other functional group is located on top of the hollow site H2 (**Fig. 2b**); Model 3 in which both functional groups are located on top of the transition metals (**Fig. 2c**); Model 4 in which one functional group is located on top of the hollow site A or B and the other functional group is located on top of the transition metals (**Fig. 2d**). The atomic coordinates are fully optimized for each type of surface functional configurations.

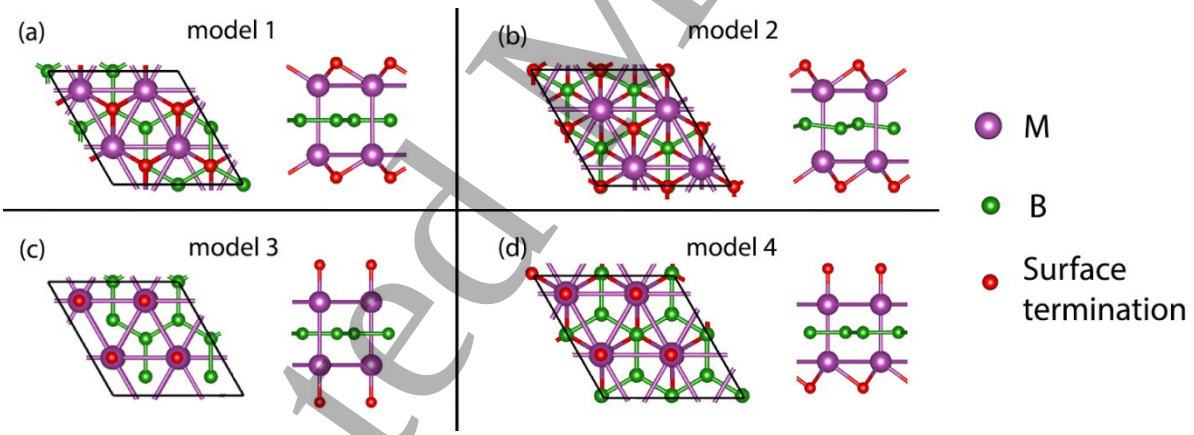

Fig. 2 Top and side views of different configuration models of the functionalized MB MBene systems. (a) model 1, (b) model 2, (c) model 3, and (c) model 4. Here, the z-direction (c-lattice direction) is the normal vector to the MBene surfaces. Hollow sites A and B are shown by blue circles in the panel (a).

4 Results and discussion

4.1 Formation energy of the 2D MBenes

The results of the total energies of optimized functionalized MBenes with different models are presented in **Supplementary information**, **Table S1**. The results show that models 1 or 2

Accepted Manuscript

are energetically more stable than the other two considered models (*i.e.*, models 3 and 4) for the MB MBene structures with different transition elements and functional groups. In most cases, after optimization, models 3 and 4 are transformed into the models 1 or 2. Our optimization results show that Model 3 is the most stable configuration only for MoB(OH), WBF, and WB(OH) MBenes.

We have next calculated the formation energies of MBene systems chemically functionalized by different functional groups in addition to pristine MBenes to find out the effect of functionalization on the stability of the MBene sheets as shown in **Table 1**. The results show that the formation energies of terminated MBenes are large negative values and these values are less negative when the transition metal changes from Sc → W. This implies that the functional groups could bond strongly to the transition metals and the possibility of the development of MBene systems with a specific surface termination. Some of the pristine MBenes possess positive values of formation energies that indicate these MBenes are thermodynamically unstable. In other words, they may transform into other competing phases at high temperatures. However, since MoB with large positive formation energy has already been obtained partially from exfoliation of Mo_2AlB_2, the other 2D MBenes might also be formed experimentally.[14] Interestingly, the formation energies of MBenes become large negative values upon surface functionalization with F, O, or OH, indicating the formation of strong bonds between termination groups and the surface. The effect of surface functionalization on the mechanical stability of the obtained 2D systems is investigated in the next subsections.

Table 1. Formation energies (eV) of different monolayer MBene systems functionalized with F, OH, and O groups in addition to pristine MBenes.

MBene Systems	Pristine	F	O	OH
ScB	-1.33	-13.26	-12.09	-11.57
TiB	-1.00	-12.00	-10.77	-10.78

Accepted Manuscript

ZrB	-1.12	-12.42	-11.34	-11.02
HfB	-1.01	-12.09	-11.92	-10.96
VB	0.17	-9.03	-8.19	-8.00
NbB	-0.02	-9.36	-9.38	-8.31
TaB	0.24	-8.64	-9.45	-7.73
MoB	1.50	-6.22	-5.84	-5.21
WB	2.34	-5.57	-5.43	-4.77

To study the effect of the exchange-correlation functional on the formation energy of the MBene systems, we have also calculated the formation energy of these systems usning HSE06 functional upon the PBE-relaxed structures.[44] The calculated results using HSE06 functional (**Table S2**, **Supplementary information**) show that the formability of these systems are even more feasible than the ones calculated using PBE functional (**Table 1**); however, the differences are relatively marginal. Note that these results are upon the PBE-relaxed structures because optimization with HSE is very heavy. Obviously, if we could relax the structures with HSE functional, the formation energies could become slightly more negative.

We have also optimized the multi-layers of the functionalized MBenes with the most stable model obtained and the results of the formation energies are presented in **Supplementary information**, **Table S3**. As stated in Introduction section and expected, the results show that the multi-layers of these 2D materials are more feasible to be produced than their monolayers in the experiments. However, there is an insignificant difference between the properties (*e.g.*, electronic) of the monolayers and multi-layers of these materials.

4.2 Dynamical Stability of MBenes

We also investigated the dynamical stability of MB MBenes by using phonon calculations. The results are provided in **Supplementary information**, **Fig. S1**. The phonon spectra of MBene systems fulfill the strictest condition for dynamical stability without imaginary

Accepted Manuscript

modes, indicating the local stability of MBenes. Among all investigated systems, we only found the negative phonon frequency in the phonon spectra of MoB(OH) and WB(OH) MBenes, as highlighted in bold-typeface in **Fig. S1**. We also found the imaginary mode in the phonon spectra of these two systems even with a larger supercell of 6 × 6 × 1. This shows that the appearance of these negative phonon frequencies is not associated with the finite size of the supercell. It is noteworthy that 2D CrB,[16,18] MoB,[13,14] and TiB[17] MBenes have already been synthesized experimentally, and consistently our calculations also confirm their stabilities. The atomic coordinates of the optimized structures are provided in **Supplementary information** for further studies by readers.

Accepted Manuscript

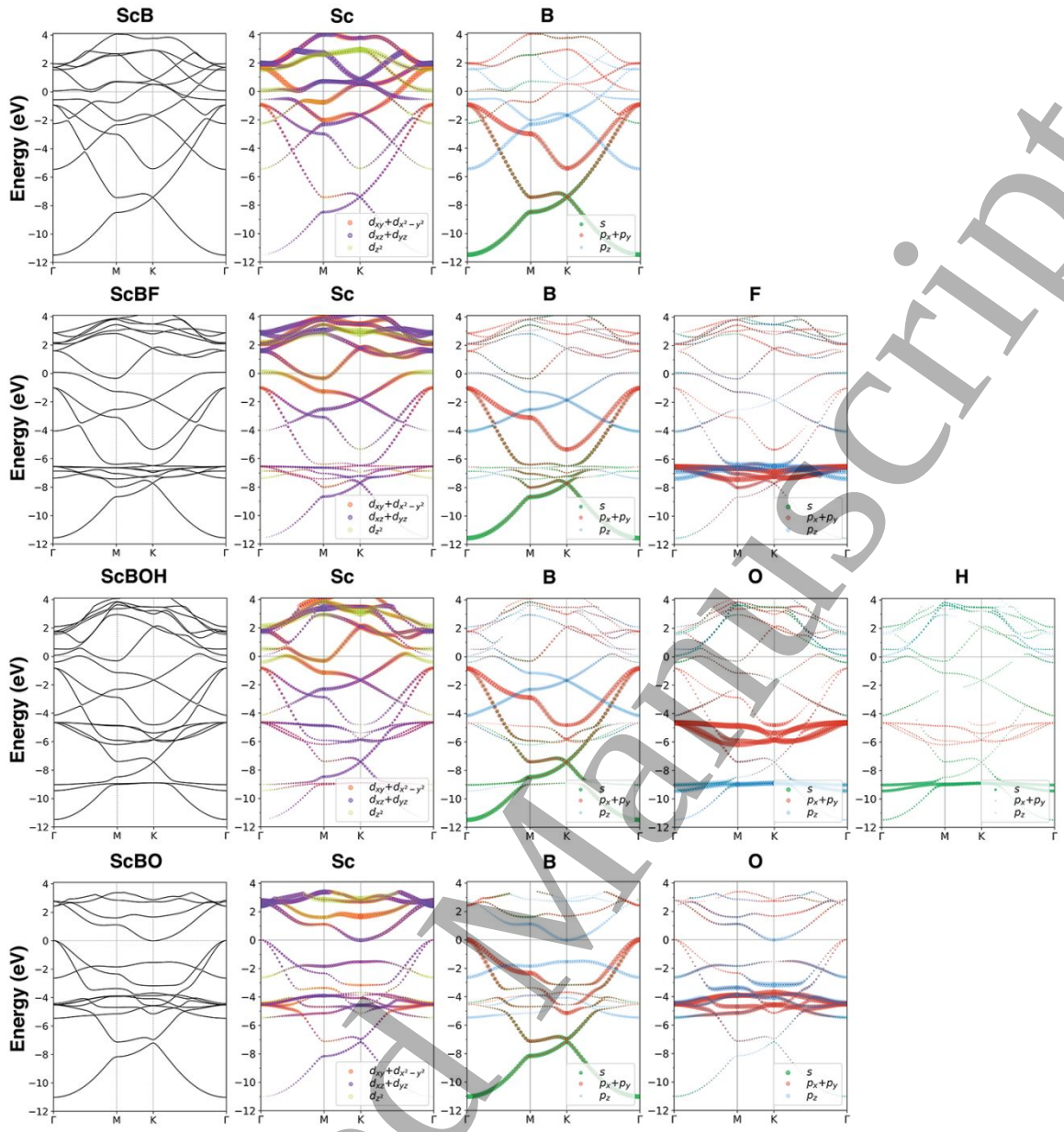

Fig. 3 Band and projected band structures of pristine ScB and functionalized ones with F, O, and OH. The Fermi energy is at zero.

4.3 Electronic structures of 2D MBenes

The crystal structures and thus the electronic structures of MBenes can be viewed from various perspectives. For example, as explained in the introduction section, 2D MB MBenes can be obtained from the exfoliation of MAB phases. Also, they can be considered as a thin film of bulk MB_2 (M = Sc, Ti, V, Nb, Ta, Mo, and W), which possesses the AlB_2 structure type

Accepted Manuscript

and the hexagonal lattice with *P6/mmm* crystallographic symmetry.[45] Furthermore, they can be considered as consecutive M-B-M layers, in which M atoms have doped the hexagonal sites of the graphene-like boron layer. The latter perspective is one of the main approaches to synthesize 2D boron-based layers. It is well known that the 2D graphene-like boron layer with the honeycomb structure is metastable. This is because unlike graphene that the 4 valence electrons of carbon atoms fill all σ and π bonding states and form a very stable 2D layer, in graphene-like boron, the three valence electrons of boron atoms can only partially occupy those bonding states.[46–48]The electron deficiencies to occupy the bonding states result in instability of the graphene-like boron layer. Hence, there is no freestanding honeycomb boron layer. To enhance the stability of the boron layer, an appropriate number of electrons should be injected into the B-B bonding states. If many electrons are injected, they occupy not only the bonding states but also the antibonding states that might result in instability of the layer again. The required electrons can be injected by adding more boron atoms[48,49] or introducing transition metals[46,47,50,51] to top of the hexagon boron rings resulting in the formation of various polyforms of boron sheets with a mixture of hexagonal and triangular boron rings. The experimental formation of various boron sheets on top of metal substrates[52] and the formation of bulk MB_2 structures evidence that the above approaches have worked well in experiments.[45]

Considering the above literature, pristine 2D MB MBenes can be viewed simply as 2D honeycomb boron layers doped with transition metals. To better understand the electronic structures of pristine and functionalized 2D MBenes, we have investigated their projected band structures. To keep the length of this paper short, we show the results for pristine and functionalized 2D ScB, TiB, VB, and MoB with F, O, and OH in **Figs. 3** and **4**, and the band structures of ZrB, HfB, NbB, TaB, and WB are included in **Supplementary information,**

Accepted Manuscript

Fig. S2. The 2D MBs (M = Sc, Ti, V, Mo) adequately represent the electronic structures of other 2D transition metal borides, whose transition metals belong to the same group — due to possessing the same number of valence electrons — in the periodic table.

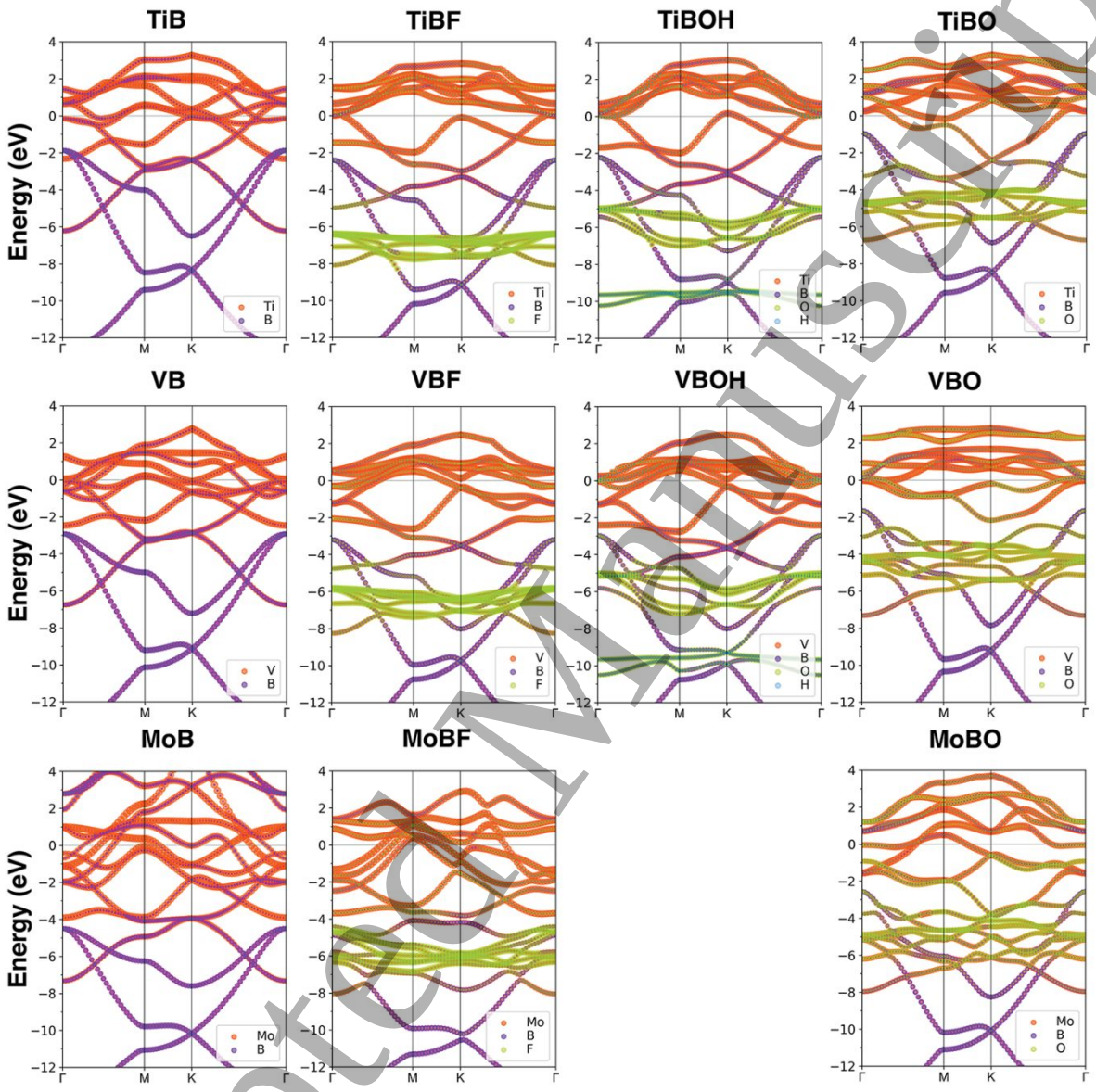

Fig. 4 Band structures of pristine MB (M = Ti, V, Mo) and functionalized ones with F, O, and OH. The Fermi energy is at zero.

As seen in **Figs. 3** and **4**, all pristine MBenes are metallic, like pristine MXenes.[2,34] For instance, the projected band structure of ScB on atomic orbitals of Sc (d_{x2-y2}+d_{xy}, d_{xz}+d_{yz}, d_{z2}) and B (s, p_x+p_y, p_z) are shown in **Fig. 3**. By considering the projected bands on Sc and B

Accepted Manuscript

atomic orbitals, it can be seen that the atomic orbitals of B atoms mainly contribute to the bands below -1 eV. The states near and above the Fermi energy result from *d* orbitals of Sc. Therefore, the metallic conductivity of 2D MBenes results from the delocalized metal *d* states. It can be seen that all *s*, p_x+p_y, p_z (p_z*) orbitals of B atoms are completely (partially) filled due to B-B atomic orbital hybridizations and by donated electrons from Sc and hybridization between Sc and B atomic orbitals. In other words, all σ and π (π*) of graphene-like boron layer have (has) been completely (partially) filled by electrons. Therefore, it can be anticipated that B-B bonds are quite strong in 2D MB MBenes but will be weaker than C-C bonds in graphene. This is because the σ bonds in graphene locate at lower energies than that in MBenes and the π* states are completely unoccupied. Moreover, since the hybridizations between atomic orbitals in B-B bonds are relatively larger than that in M-B, it can be expected that the B-B bonds are stronger than the M-B bonds. It is seen that the largest hybridization between Sc and B occurs when p_z and p_z* orbitals of B atoms overlap with d_{xz}+d_{yz} orbitals of Sc by filling the π and π* states of boron atoms. The π and π* bands cross each other at -2 eV at K point of the Brillouin zone, which is analogous to graphene can be considered as the Dirac point for the boron layer in MBenes. As seen from the projected band structures, there are few occupied transitions metal bands below the Fermi energy compared to boron-related bands. Therefore, it is generally expected that in a 2D MB MBene, M-M bonds will be weaker than both B-B and M-B bonds. It can be predicted that among 2D MB MBenes, the ScB (MoB and WB) possess the weakest (strongest) M-M bonds because it (they) has (have) one (four) occupied Sc (Mo and W) *d* band(s).

In pristine 2D MB MBene, when the transition metal changes from Sc → W, because the number of valence electrons increases, consequently more *d* bands become occupied and shift to below the Fermi energy and simultaneously the σ, π, and π* bands of B shift to lower

Accepted Manuscript

energies indicating the B-B bonds get stronger. It can be anticipated that the B-B bonds in MoB and WB are the strongest in pristine MBenes.

To investigate the effect of F, OH, or O functionalization on electronic structures of pristine MB MBenes, we have shown the bands and projected bands of ScBT (T = F, OH, or O) in **Fig. 3** and the projected band structures of MBT (M = Ti, V, Mo; T = F, OH, O) in **Fig. 4**. By comparing the projected band structures of MBF, MBOH and MBO with pristine MB, it can be realized that since the electronegativity of F, OH, or O is higher than the studied transition metals, these termination groups affect the electronic structures in two ways: 1) popping out the electrons partially/completely from the occupied *d* bands below the Fermi energy and/or from the π* band states of boron atoms, 2) hybridizing with *d* orbitals of transition metals and forming new states at energies deep below the Fermi energy. About the latter effect, the states, resulting from hybridization between Sc *d* orbitals and F (O) *p* orbitals are formed around -8 (-5) eV. The O-H bond states locate around -9 eV. About the former effect, since the surfaces of 2D MBenes are fully saturated with 2 F or 2 O groups, they can pop out 2 or 4 electrons from the occupied states, respectively. In other words, due to saturation with F or O, effectively one or two bands become unoccupied near the Fermi energy, respectively. By comparing the projected band structures of ScBF and ScBO with pristine ScB, it is seen that F groups unoccupied one of the top Sc *d* valence bands and simultaneously the band curvatures of other bands near the Fermi energy change such that ScBF becomes a semimetal system. Similarly, in other 2D MBF MBenes, it is seen that the M *d* bands (the π* bands of B atoms) become mostly (partially) unoccupied.

Since both F and OH chemical groups need one electron to completely fill their valence shell, in general, the electronic structures of F and OH terminated MBenes are similar. However,

Accepted Manuscript

due to positively charged surfaces of OH terminated MBenes, some new surface states are created, known as nearly free electron (NFE) states that are found near or at the Fermi energy at the Gamma point with parabolic-like curvature. For instance, the NFE state in ScBOH is exactly above the Fermi level at the Gamma point. The formation of such NFE states has already been well investigated and explained for OH-terminated MXenes.[53,54] The same theory is applicable to the case of OH-terminated MBenes.

In the case of O termination of ScB, two top valence bands of ScB become unoccupied: the top Sc *d* band and the π* band of boron atoms. This results in the semimetal behavior of ScBO. The same scenario is true for the oxidation effect of the other pristine 2D MBs (M = Ti, Zr, Hf, V, Nb, Ta, Mo, W). However, the above pristine MB MBenes have more occupied M *d* bands below the Fermi energy than that in ScB. Hence, when they are terminated with O, the M *d* bands (the π* band of boron atoms) will mostly (partially) become unoccupied. Among the studied systems, ScBF, ScBOH, ScBO, ZrBO, and HfBO are semimetal. It is known that GGA functionals underestimate the band gaps. Hence, we have investigated the band structures of these systems using the HSE06 method.[44] We found that only ScBO becomes an indirect bandgap semiconductor with a 0.5 eV gap while others remain semimetallic.

If we carefully look at the band structures of TiBF, ZrBF, and HfBF, it is realized that the $d_{x^2-y^2}$+d_{xy} and d_{xz}+d_{yz} bands of the transition metals are touched near the Fermi energy and form tilted Dirac-cones near the Gamma point. Therefore, these systems might be interesting for investigating emergent Dirac fermions.[55–58] Just recently, Shang *et al.* performed a detailed analysis on the electronic structures of TiBF.[59] They indicated that TiBF is a metallic system hosting the coexistence of type-I and type-II nodal line band crossings close to the Fermi

Accepted Manuscript

level. Here, we have followed the same band analysis as performed by Shang *et al.*[59]. It is demonstrated that ZrBF and HfBF show similar band topologies near the Fermi as TiBF. In detail, we have depicted the band structures of TiBF, ZrBF, and HfBF without spin-orbit (SOC) coupling in **Fig. 5a**. The band structures of these systems have also calculated with SOC effect, as shown in **Supplementary information**, **Fig. S3**. It is seen that some of the electron-like bands (labeled α, β or η) and/or hole-like ones (labeled γ) cross each other near the Fermi level and form Dirac-like cones at finite points indicated by circles. Considering the band dispersion slope, the Dirac cones can be classified into type-I or type-II. The type-I (type-II) represents the convectional (tilted) Dirac conical band dispersions in which the energy spectrums of the electron and hole states are well separated (coexist at a given energy).[60,61] To better imagining the band crossing features, we have plotted the 3D band dispersions of ZrBF in **Fig. 5b**. It is clearly seen that the type I or II band crossings form some rings known as nodal rings in the Brillouin zone centered around Γ point. Since, TiBF, ZrBF, and HfBF are nonmagnetic, the time-reversal symmetry is protected. However, they do not possess space inversion symmetry. The emergence of the nodal rings results from the mirror symmetries in these structures. The mirror (M_z) band parities of α, β, η and γ states are shown in **Fig. 5**. The +/- sign indicates the even/odd parity. When the bands with the same (opposite) parities cross with each other, they will (will not) open a gap. For example, in ZrBF, the electron-like bands of α and β (having even parities) cross the hole-like band of γ (having an odd parity) without opening a bandgap, resulting in the formation of two nodal rings. Upon including the spin-orbit (SOC) coupling, the number of bands becomes double. The states with the same parity form small band gaps less than 22 meV by lifting the degeneracies of the states at nodal rings. Shang *et al.* have further demonstrated that upon applying an appropriate biaxial strain, it is possible to drive TiBF to turn into a 2D semiconductor, Weyle semimetal, or a nodal metal.[59]

Accepted Manuscript

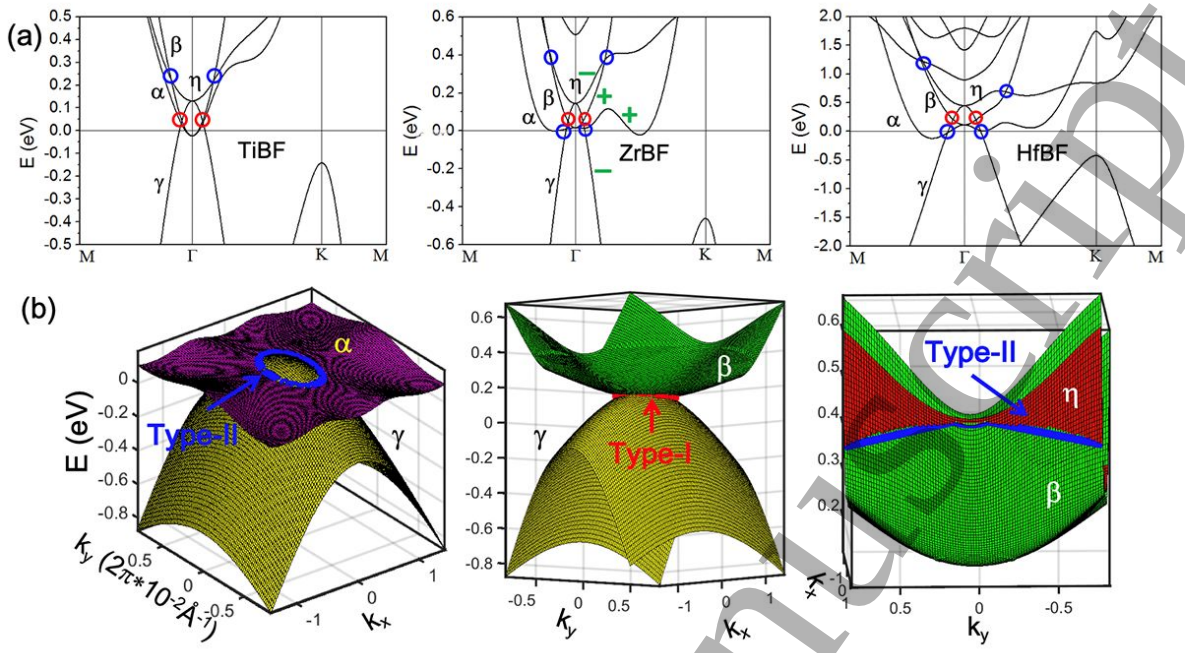

Fig. 5 (a) The band structures of TiBF, ZrBF, and HfBF calculated without spin-orbit-coupling (SOC) effect. The red and blue circles indicate the type-I and type-II Dirac band dispersions, respectively. The "+" ("-") represents the Mz parity of the band. (b) 3D band structures of ZrBF showing the cross-sections of α, β, η and γ bands.

It is noteworthy that some of the functionalized MBenes such as ScBF, MoBO, and WBO have a partially flat band state near the Fermi energy that is mainly contributed by d_{z2} orbitals of the metals. These materials with such peculiar band structures may possess large Seebeck coefficients because they are semimetals or metals possessing relatively good electrical conductivity. Therefore, they might be promising candidates for thermoelectric applications[62] or flat band physics.[63,64]

4.4 Bond strength of MBenes

To understand the mechanical properties in the next subsection better, we have studied the strength of B-B, M-M, and M-B bonds in all studied MBenes using ICOHP and force

Accepted Manuscript

constants calculations, as shown in **Fig. 6**. For the functionalized MBenes, besides, we have also calculated those quantities for the M-T bonds (T= F, O, and OH).

As explained in the section of computational methods, the integrated COHP (ICOHP) and force constant are employed to determine the bond strength. In chemistry, the bond strength of a covalent interaction is mainly dependent on an orbital overlap of the two adjacent atoms that form a bond. Typically, the bond length is affected by this orbital overlap, which the more overlap would provide the shorter bond length. We calculated the integrated COHP (ICOHP) up to the Fermi energy over all the atomic orbital interactions between the atoms forming the bonds, which has also been applied to MAX and MAB phases.[15,19] In the literature, the strength of a bond can be measured using force constant calculations if atoms are connected by spring.[15,19,65] The quantity of the force constant is calculated in terms of the second derivative (first derivative) of the total energy (force) regarding the displacement of an atom. We performed the phonon calculations on the considered MBenes (see **Fig. S1**) to investigate the force constants of the bonds in MBenes. As shown in **Fig. 6**, the stiffest and weakest bondings are between B-B and M-M atoms in MBenes, which is compatible with that observed in MAB phases[15] and the results of electronic structure calculations discussed in the previous subsection. Generally, as the atom-atom distance increases, the force constants, and bond strength decreases (**Figs. 6a** and **6b**). It is perceived in **Fig. 6c** that there is a correlation between the force constant and the strength of bonds so that the force constant increases with the increasing bond strength. The results, generally speaking, illustrate relatively similar trends for both quantities, in which the bond strength is weaker in larger atom-atom distances. In general, the strength of the bonds shows the following trend in MBenes when their structure models are the same: B-B > M-O > M-F ≈ M-OH > M-B> M-M bonds. Therefore, as expected and will be proved in the next section, due to the formation of strong M-T (T= F, OH, or O), the mechanical properties of MBenes are enhanced.

Accepted Manuscript

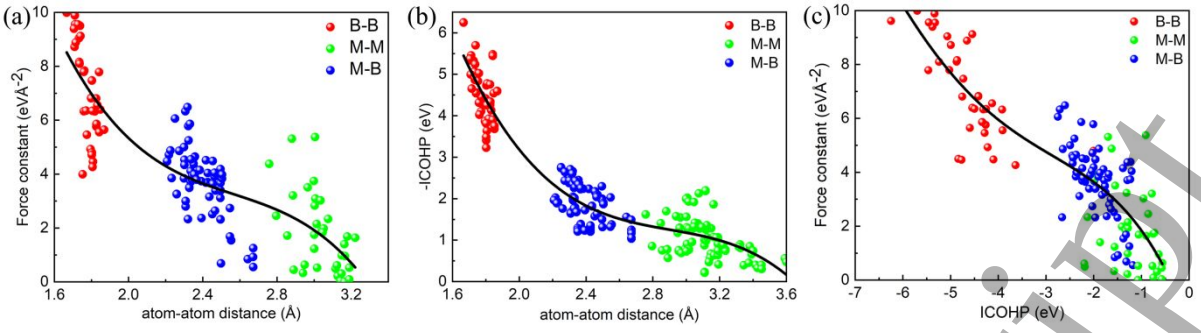

Fig. 6 Calculated (a) force constants and (b) bond strength versus atom-atom distance, and (c) force constants versus bond strength for the B-B, M-M, and M-B bonds for all considered MBenes. The bond strength is calculated by the integrated crystal orbital Hamilton population (ICOHP) up to the Fermi energy over all the atomic orbital interactions between the atoms forming the bonds. The solid lines indicate the polynomial fit to the results.

To see the effect of the surface functionalization on the bond strength of MBenes in more detail, the results of force constant and ICOHP versus bond distance for pristine MBenes and chemically functionalized by F, O, and OH are shown separately in **Supplementary information**, **Figs. S4(a-l)**. The bond strength analyses indicate that the B-B bonds are stronger than other bonds in all MBene structures and O functional groups make the bindings between B-B (M-M) stiffer (weaker) in MBenes. This can be well understood from the results of projected band structures. As explained before, oxidation of MBenes removes electrons from π* band (antibonding state) of graphene-like boron layer and transition metal *d* bands. This results in the strengthening and weakening of the B-B and M-M bonds, respectively.

4.5 Mechanical Properties of MBenes

To understand the mechanical properties of MBenes, we further calculated the elastic constants (c_{11} and c_{12}), Poisson's ratio, shear modulus, and Young's modulus of MBenes by using a Taylor expansion of the total energy of the MBene systems regarding a small strain of the lattice, which is well explained in Ref.[66]. Since our phonon calculations (see **Fig. S1**)

Accepted Manuscript

imply that MoB(OH) and WB(OH) MBenes are not dynamically stable, we exclude these two systems from our discussion.

The results of elastic constant calculations (c_{11} and c_{12}) of MBenes are summarized in **Table 2 and shown in Figs. 7a** and **7b**. The results generally indicate that MBenes terminated by oxygen exhibit larger elastic constants as compared to MBenes functionalized with F or OH. This is consistent with the results of MXenes and is attributed to the stronger bonding between the oxygen atoms and surface transition metals.[2,34,67,68] The results imply that functionalized MBenes (excluding MoB and WB) are mechanically stiffer than the associated pristine MBenes. Like the MBenes, it was predicted that surface terminations make MXenes mechanically stiffer than the associated pristine MXenes.[42]

Table 2. Calculated elastic constants (c_{11} and c_{12}) of different MBene systems functionalized with F, OH, and O groups in addition to pristine MBenes. The values are in N/m.

MBene Systems	Pristine		F		O		OH	
	c_{11}	c_{12}	c_{11}	c_{12}	c_{11}	c_{12}	c_{11}	c_{12}
ScB	207.78	18.18	255.32	39.57	267.95	74.17	256.02	38.86
TiB	230.52	32.38	274.38	62.12	353.56	94.78	296.44	48.66
ZrB	220.72	46.52	236.88	62.59	324.19	87.64	266.78	43.17
HfB	240.96	56.96	287.59	50.31	353.85	89.59	294.50	39.98
VB	217.92	54.20	257.71	62.42	336.97	118.68	238.10	44.55
NbB	208.77	86.44	238.45	68.87	338.96	126.16	230.24	49.50
TaB	236.22	81.73	242.47	73.02	354.15	115.66	226.78	59.85
MoB	250.07	45.67	200.97	31.89	280.82	36.65	-	-
WB	296.52	63.11	208.23	45.01	354.41	49.55	-	-

The Poisson's ratio, which is a ratio of transverse contraction to the longitudinal expansion of the lattice in the direction of stretching force, is calculated by the formula $\nu = \frac{c_{12}}{c_{11}}$. The results (**Fig. 7c**) show that the Poisson's ratio varies between 0.087 and 0.414. This ratio is higher

Accepted Manuscript

for the MBenes terminated by oxygen with the transition metal changing from Sc → V while pristine MBenes with the transition metal changing from Nb → W possess the highest Poisson's ratio. Comparing the Poissons's ratio of the MBenes terminated by fluorine and hydroxide indicates that fluorine surface terminations provide the higher Poisson's ratio than hydroxide functional groups.

The shear modulus refers to the material's response to shear stress and a large (small) shear modulus value indicates that the rigidness (softness) of a system to cutting, e.g., with dull scissors. The results of the calculated shear modulus (**Fig. 7d**) generally show that a larger force is required to produce deformation in the MBenes terminated by oxygen or F while pristine MBenes (excluding MoB and WB) would be deformed by a smaller force. In other words, the pristine MBenes are in general more ductile than the functionalized one, like the MXenes, which was predicted to become more mechanically stiffer after surface functionalizations.[67,68]

The Young's modulus describes the material's strain response to uniaxial stress in the direction of this stress like pulling. It is calculated by the formula $E = \frac{(c_{11})^2 - (c_{12})^2}{c_{11}}$. The results for MBenes are shown in **Fig. 7e**. Among the MBene systems, oxygen terminated MBenes exhibit the stiffest mechanical strength with 248 < E (N/m) < 348, and pristine MBenes are the weakest systems with 206 < E (N/m) < 283. It is predicted that any type of surface terminations (F, O, and OH) could enhance Young's modulus for all the considered MBenes with the transition metal changing from Sc → W. However, our results indicate that fluorine functional groups could make MoB and WB MBenes mechanically weaker than the associated pristine MBenes. To estimate Young's modulus of MBene monolayers in GPa, we calculated the thickness of MBene flakes by optimizing the multilayer MBenes. The thickness of MBene monolayers was predicted in the range of 0.8 to 1.0 nm, which resulted in Young's modulus of MBenes in the range of 200-320 GPa. By comparing the considered

Accepted Manuscript

MBenes with the MXenes predicted to have high Young's modulus in the range of 400-1000 GPa,[1,2,34,67,68,70–72] depending on the composition, surface terminations, and the number of layers, it can be concluded that the considered MBenes are weaker than the MXenes.

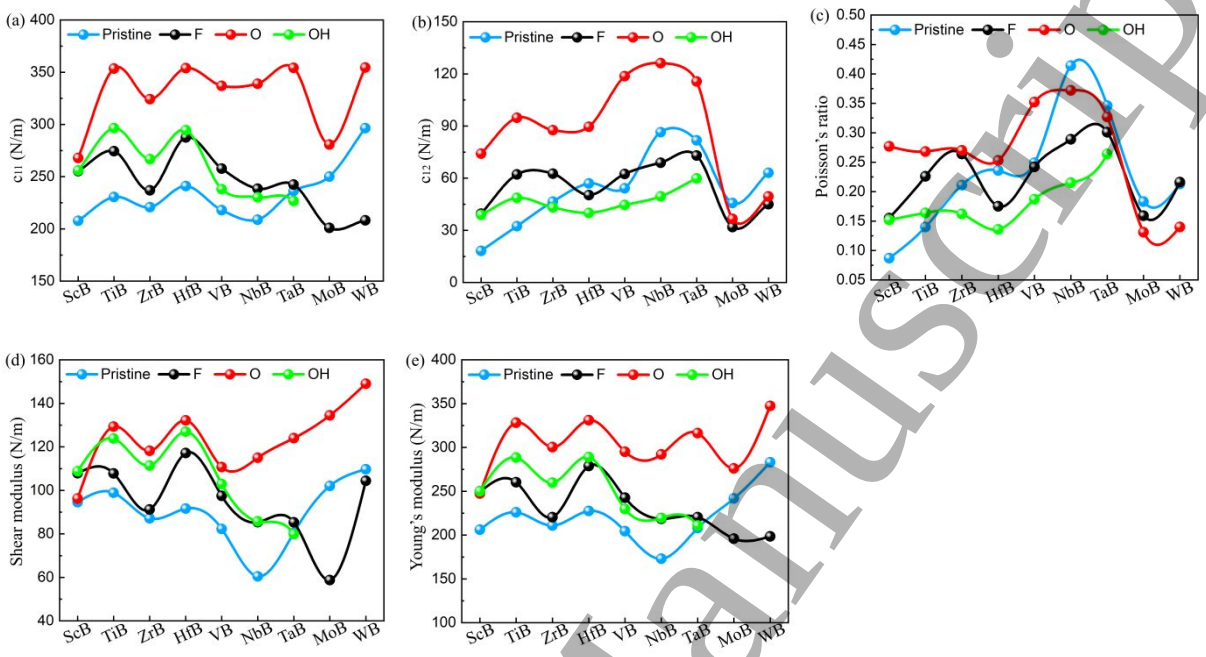

Fig. 7 Calculated mechanical properties of MBene systems. The elastic constants of (a) c_{11} and (b) c_{22}. (c) Poisson's ratio, (d) Shear modulus, and (e) Young's modulus.

Electron work function of MBenes

We calculated the work function of MBenes, which provides information on the minimum energy required to extract an electron from the Fermi level to a region outside the crystal. The work function is a very important parameter in designing new electronic devices, electron emitters, and Schottky barriers.[73] It is calculated as the energy difference between the electrostatic potential at an infinite distance of crystal and its Fermi energy. **Fig. 8** shows the calculated electron work function of considered MBenes. The results indicate that the electron work function in MBenes terminated by O is the highest and this quantity is the lowest in MBenes terminated by OH. Similar to MXenes, the ultralow work functions of OH terminated MBenes can be attributed to the polarity of OH groups.[74] It seems that V, Mo, and W MBenes functionalized with F or O possess the highest work function.

Accepted Manuscript

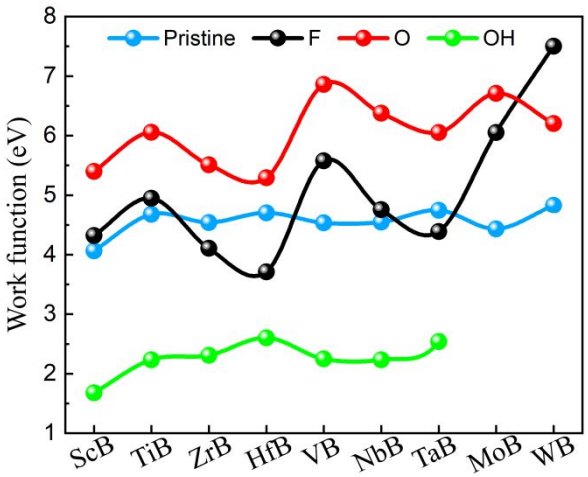

Fig. 8 Calculated electron work function of MBene systems.

5 Conclusion

The family of transition 2D transition metal borides, named as MBene, with hexagonal or orthorhombic phases is developing rapidly. Here, we have focused on the electronic structure of hexagonal 2D MBenes and planned to investigate the orthorhombic ones in the future. In detail, we theoretically predicted the structural stabilities and mechanical properties of the hexagonal monolayer of non-terminated and terminated MB MBenes (M = Sc, Ti, Zr, Hf, V, Nb, Ta, Mo, and W) with F, O, or OH groups using DFT at absolute zero temperature. After finding the most stable structural models, the formation energy of the most stable geometries has been calculated and the results indicate the great potential of strong bonding between the functional groups and the surface transition metals and the possibility of the development of MBenes with those surface terminations. The dynamical stability of considered MBenes has also been analyzed employing phonon calculations and the results show that most pristine and functionalized 2D MB MBenes are stable. We further investigated the work functions of MBenes and the results, generally, indicate that O terminations provide the highest energy barrier for electron emission, while MBenes terminated by OH have the lowest energy barrier. The calculations of the mechanical properties indicate that the considered MBenes are generally weaker than the MXenes. Furthermore, the bond strength analyses indicate that in all pristine or functionalized MBenes, the B-B bonds are stronger than M-B > M-M bonds.

Accepted Manuscript

The termination groups (T= F, O, and OH) form strong bonds with the surface transition metals such that M-T bonds are stronger than M-B or M-M bonds resulting in enhanced mechanical stabilities of functionalized MBenes compared to the pristine ones. Moreover, the MBenes terminated by O are mechanically the stiffest and the most flexible systems while non-terminated MBenes are generally the weakest and the most brittle systems as compared to other MBenes. Therefore, like MXenes, it is predicted that surface terminations make MBenes stiffer. We hope this study will motivate new theoretical and experimental researches on 2D MBenes.

Conflicts of interest

There are no conflicts to declare.

Acknowledgments

The authors would like to acknowledge and greatly appreciate the financial support from VISTA which is a basic research program in collaboration between the Norwegian Academy of Science and Letters, and Equinor. The authors would also like to thank the Department of Mechanical and Industrial Engineering at the Norwegian University of Science and Technology (NTNU). The authors also acknowledge generous grants of high-performance computer time from both Vilje and UNINETT Sigma.

References

1 B. Anasori, M. R. Lukatskaya and Y. Gogotsi, *Nat. Rev. Mater.*, 2017, **2**, 16098.
2 M. Khazaei, A. Ranjbar, M. Arai and S. Yunoki, *J. Mater. Chem. C*, 2017, **5**, 2488–2503.
3 M. W. Barsoum, *Prog. Solid St. Chem.*, 2000, **28**, 201–281.
4 M. Khazaei, M. Arai, T. Sasaki and M. Estili, *J. Phys. Condens. Matter*, 2014, **26**, 505503.
5 M. Khazaei, M. Estili, N. S. Venkataramanan, T. Sasaki, Y. Sakka, C. Chung, M. Arai and Y. Kawazoe, *Adv. Funct. Mater.*, 2013, **23**, 2185–2192.
6 M. W. B. M. Naguib, O. Mashtalir, J. Carle, V. Presser, L. Hultman, Y. Gogotsi, *ACS Nano*, 2012, **6**, 1322–1331.
7 Q. Tao, M. Dahlqvist, J. Lu, S. Kota, R. Meshkian, J. Halim, J. Palisaitis, L. Hultman, M. W. Barsoum, P. O. Å. Persson and J. Rosen, *Nat. Commun.*, 2017, **8**, 14949.
8 M. Khazaei, V. Wang, C. Sevik, A. Ranjbar, M. Arai and S. Yunoki, *Phys. Rev. Mater.*, 2018, **2**, 074002.
9 M. Dahlqvist, A. Petruhins, J. Lu, L. Hultman and J. Rosen, *ACS Nano*, 2018, **12**, 7761–7770.
10 A. Champagne, F. Ricci, M. Barbier, T. Ouisse, D. Magnin, S. Ryelandt, T. Pardoen, G. Hautier, M. W. Barsoum and J. Charlier, *Phys. Rev. Mater.*, 2020, **4**, 13604.
11 B. Anasori, Y. Xie, M. Beidaghi, J. Lu, B. C. Hosler, L. Hultman, P. R. C. Kent, Y. Gogotsi and M. W. Barsoum, *ACS Nano*, 2015, **9**, 9507–9516.
12 M. Ade and H. Hillebrecht, *Inorg. Chem.*, 2015, **54**, 6122–6135.
13 L. T. Alameda, C. F. Holder, J. L. Fenton and R. E. Schaak, *Chem. Mater.*, 2017, **29**, 8953–8957.
14 L. T. Alameda, P. Moradifar, Z. P. Metzger, N. Alem and R. E. Schaak, *J. Am. Chem. Soc.*, 2018, **140**, 8833–8840.
15 M. Khazaei, J. Wang, M. Estili, A. Ranjbar, S. Suehara, M. Arai, K. Esfarjani and S. Yunoki, *Nanoscale*, 2019, **11**, 11305–11314.
16 H. Zhang, H. Xiang, F. Dai, Z. Zhang and Y. Zhou, *J. Mater. Sci. Technol.*, 2018, **34**, 2022–2026.
17 J. Wang, T. N. Ye, Y. Gong, J. Wu, N. Miao, T. Tada and H. Hosono, *Nat. Commun.*, 2019, **10**, 2284.
18 H. Zhang, F. Dai, H. Xiang, X. Wang, Z. Zhang and Y. Zhou, *J. Matererial Sci. Technol.*, 2019, **35**, 1593–1600.

Accepted Manuscript

19 M. Khazaei, A. Ranjbar, K. Esfarjani and D. Bogdanovski, *Phys. Chem. Chem. Phys.*, 2018, **20**, 5879–5892.

20 F. Shahzad, M. Alhabeb, C. B. Hatter, B. Anasori, S. M. Hong, C. M. Koo and Y. Gogotsi, *Science (80-.).*, 2016, **353**, 1137–1140.

21 A. Sarycheva, A. Polemi, Y. Liu, K. Dandekar, B. Anasori and Y. Gogotsi, *Sci. Adv.*, 2018, **4**, eaau0920.

22 C. E. Ren, M. Alhabeb, B. W. Byles, M. Zhao, B. Anasori, E. Pomerantseva, K. A. Mahmoud and Y. Gogotsi, *ACS Appl. Nano Mater.*, 2018, **1**, 3644–3652.

23 M. Ghidiu, M. R. Lukatskaya, M. Zhao, Y. Gogotsi and M. W. Barsoum, *Nature*, 2014, **516**, 78–81.

24 M. R. Lukatskaya, O. Mashtalir, C. E. Ren, Y. D. Agnese, M. W. Barsoum and Y. Gogotsi, *Science (80-.).*, 2013, **341**, 1502–1506.

25 M. Zhao, X. Xie, C. E. Ren, T. Makaryan, B. Anasori, G. Wang and Y. Gogotsi, *Adv. Mater.*, 2017, **29**, 1702410.

26 M. Zhao, M. Torelli, C. E. Ren, M. Ghidiu, Z. Ling, B. Anasori, M. W. Barsoum and Y. Gogotsi, *Nano Energy*, 2016, **30**, 603–613.

27 R. Khaledialidusti, A. K. Mishra and A. Barnoush, *J. Mater. Chem. C*, 2020, **8**, 4771–4779.

28 G. Gao, P. Sun, Y. Li, F. Wang, Z. Zhao, Y. Qin and F. Li, *ACS Catal.*, 2017, **7**, 494–500.

29 Z. Ma, F. Sun, M. Dou, Q. Yao, Y. Liu and F. Wu, *Phys. Lett. A*, 2020, 126282.

30 Z. Guo and Z. Sun, *J. Mater. Chem. A*, 2017, **5**, 23530–23535.

31 G. Yuan, T. Bo, X. Qi, P. Liu and Z. Huang, *Appl. Surf. Sci.*, 2019, **480**, 448–453.

32 T. Bo, P. Liu, B. Wang and J. Zhang, *Phys. Chem. Chem. Phys.*, 2019, **21**, 5178–5188.

33 Z. Jiang, P. Wang and X. Jiang, *Nanoscale Horiz.*, 2018, **3**, 335–341.

34 M. Khazaei, A. Mishra, N. S. Venkataramanan, A. K. Singh and Y. Seiji, *Curr. Opin. Solid State Mater. Sci.*, 2019, **23**, 164–178.

35 C. L. Bailey, S. Mukhopadhyay, A. Wander, B. G. Searle and N. M. Harrison, *J. Phys. Chem. C*, 2009, **113**, 4976–4983.

36 S. Mukhopadhyay, C. L. Bailey, A. Wander, B. G. Searle and C. A. Muryn, *Surf. Sci.*, 2007, **601**, 4433–4437.

37 J. P. Perdew, K. Burke and M. Ernzerhof, *Phys. Rev. Lett.*, 1996, 3865–3868.

38 G. Kresse and J. Furthmiiller, *Comput. Mater. Sci.*, 1996, **6**, 15–50.

39 H. J. Monkhorst and J. D. Pack, *Phys. Rev. B Solid State*, 1976, 5188–5192.

40 M. Methfessel and A. T. Paxton, *Phys. Rev. B*, 1989, **40**, 3616–3621.

41 A. Togo, F. Oba and I. Tanaka, *Phys. Rev. B*, 2008, **78**, 134106.

42 Y. Liu, K. T. E. Chua, T. C. Sum and C. K. Gan, *Phys. Chem. Chem. Phys.*, 2014, **16**, 345–350.

43 R. Dronskowski and P. E. Blochl, *J. Phys. Chem.*, 1993, **97**, 8617–8624.

44 J. Heyd, G. E. Scuseria and M. Ernzerhof, *J. Chem. Phys.*, 2003, **118**, 8207–8215.

45 G. Akopov, M. T. Yeung and R. B. Kaner, *Adv. Mater.*, 2017, **29**, 1604506.

46 S. Xie, X. Li, Q. Tian, N. Chen and Y. Wang, *Phys. Chem. Chem. Phys.*, 2014, **17**, 1093–1098.

47 H. Tang, S. Ismail-beigi and B. Mgb, *Phys. Rev. B*, 2009, **80**, 134113.

48 H. Tang and S. Ismail-beigi, *Phys. Rev. Lett.*, 2007, **99**, 115501.

49 X. Wu, J. Dai, Y. Zhao, Z. Zhuo, J. Yang and X. C. Zeng, *ACS Nano*, 2012, **6**, 7443–7453.

50 J. Yu, M. Khazaei, N. Umezawa and J. Wang, *J. Mater. Chem. C*, 2018, **6**, 5803–5811.

51 J. Wang, M. Khazaei, M. Arai, N. Umezawa, T. Tada and H. Hosono, *Chem. Mater.*, 2017, **29**, 5922.

52 Z. Zhang, E. S. Penev and B. I. Yakobson, *Chem. Soc. Rev.*, 2017, **46**, 6746.

53 J. Zhou, M. Khazaei, A. Ranjbar, V. Wang, T. D. Kühne, K. Ohno, Y. Kawazoe and Y. Liang, *arXiv Prepr. arXiv1912.03054*.

54 M. Khazaei, A. Ranjbar, M. Ghorbani-asl, M. Arai, T. Sasaki, Y. Liang and S. Yunoki, *Phys. Rev. B*, 2016, **93**, 205125.

55 C. Si, K. Jin, J. Zhou, Z. Sun and F. Liu, *Nano Lett.*, 2016, **16**, 6584–6591.

56 Y. Liang, M. Khazaei, A. Ranjbar, M. Arai, S. Yunoki and Y. Kawazoe, *Phys. Rev. B*, 2017, **96**, 195414.

57 M. Khazaei, A. Ranjbar, M. Arai and S. Yunoki, *Phys. Rev. B*, 2016, **94**, 125152.

58 H. Weng, A. Ranjbar, Y. Liang, Z. Song, M. Khazaei, S. Yunoki, M. Arai, Y. Kawazoe, Z. Fang and X. Dai, *Phys. Rev. B*, 2015, **92**, 075436.

59 J. Shang, Y. Liang, L. Yang, J. Li and D. Liang, *Solid State Commun.*, 2020, **310**, 113839.

Accepted Manuscript

60 S. Yalameha and N. Zahra, *J. Phys. Condens. Matter Pap.*, 2020, **32**, 295502.

61 S. Yang, H. Yang, E. Derunova, S. S. P. Parkin, B. Yan, M. N. Ali, H. Yang, E. Derunova, S. S. P. Parkin and B. Yan, *Adv. Phys. X*, 2018, **6149**, 1–29.

62 M. Khazaei, M. Arai, T. Sasaki, M. Estili and Y. Sakka, *Phys. Chem. Chem. Phys.*, 2014, **16**, 7841.

63 Y. W. Choi and H. J. Choi, *Phys. Rev. B*, 2019, **100**, 201402.

64 P. Lucignano, D. Alf, V. Cataudella, D. Ninno, G. Cantele, M. S. Angelo and C. Napoli, *Phys. Rev. B*, 2019, **99**, 195419.

65 K. Brandhorst and J. Grunenberg, *Chem. Soc. Rev.*, 2008, **37**, 1558–1567.

66 L. Fast, J. M. Wills, B. Johansson and O. Eriksson, *Phys. Rev. B*, 1995, **51**, 17431–17438.

67 Z. Guo, J. Zhou, C. Si and Z. Sun, *Phys. Chem. Chem. Phys.*, 2015, **17**, 15348–15354.

68 Z. H. Fu, Q. F. Zhang, D. Legut, C. Si, T. C. Germann, T. Lookman, S. Y. Du, J. S. Francisco and R. F. Zhang, *Phys. Rev. B*, 2016, **94**, 1–10.

69 R. Khaledialidusti, B. Anasori and A. Barnoush, *Phys. Chem. Chem. Phys.*, 2020, **22**, 3414–3424.

70 G. Plummer, B. Anasori, Y. Gogotsi and G. J. Tucker, *Comput. Mater. Sci.*, 2019, **157**, 168–174.

71 N. Zhang, Y. Hong, S. Yazdanparast and M. A. Zaeem, *2D Mater.*, , DOI:10.1088/2053-1583/aacfb3.

72 A. Lipatov, H. Lu, M. Alhabeb, B. Anasori, A. Gruverman, Y. Gogotsi and A. Sinitskii, *Sci. Adv.*, 2018, **4**, eaat0491.

73 Y. Liu, H. Xiao and W. A. Goddard, *J. Am. Chem. Soc.*, 2016, **138**, 15853−15856.

74 M. Khazaei, M. Arai, T. Sasaki, A. Ranjbar, Y. Liang and S. Yunoki, *Phys. Rev. B*, 2015, **92**, 075411.

Accepted Manuscript